Separation and characterization of cellulose nanocrystals by multi-detector asymmetrical-flow field-flow fractionation

Arnab Mukherjee and Vincent A. Hackley

Materials Measurement Science Division, National Institute of Standards and Technology, 100 Bureau Drive Stop 8520, Gaithersburg, Maryland 20899-8520, USA

Abstract: Cellulose nanocrystals (CNCs) are renewable, naturally derived polymeric nanomaterials receiving substantial attention for a wide range of potential applications. The recent availability of high quality reference materials will facilitate the development and validation of measurement methods needed to advance the scientific and commercial use of CNCs. In the present study, we demonstrate an optimized method to fractionate CNCs with narrow size dispersion based on asymmetrical-flow field-flow fractionation (AF4) coupled with on-line multi-angle light scattering (MALS), dynamic light scattering (DLS), and differential refractometry (dRI). A stable suspension of CNC (Certified Reference Material CNCD-1, National Research Council-Canada) in deionized water was prepared using a dispersion method provided by NRC and adopted from a protocol originally developed at the National Institute of Standards and Technology. The as-prepared material was initially characterized in batch mode to validate the NCR dispersion method. AF4 was then optimized for channel and cross flow, mobile phase composition, and injection volume, among other parameters. Additionally, suspensions containing (1.25 – 10) mg/mL CNC were injected directly into the dRI detector (off-line), yielding a *dn/dc* value of 0.148 ± 0.003 mL/g. dRI was then used as an on-line mass sensitive detector to quantify recovery. Results show that maximum recovery (≈ 99 %) was achieved under optimized conditions. The weight-averaged molar mass (M_w) was estimated at roughly 10^7 Da from a partial Zimm analysis. The optical radius of gyration, R_g, and the hydrodynamic radius, R_h, were measured during elution. The shape factor (R_g/R_h) ranged from 1.5 to 1.9 for the fractionated material, supporting an elongated or rod-like structure. To our knowledge, this is the first time that both the morphology and molar mass of CNCs have been directly measured for the full distribution of species. Finally, we developed and demonstrated a semi-preparatory fractionation method to separate CNCs at the milligram scale for off-line research and analysis.

Keywords: cellulose nanocrystal, hydrodynamic size, radius of gyration, shape factor, asymmetric flow field-flow fractionation, nanomaterial, nanometrology, natural product

Introduction:

Renewable and biocompatible nanomaterials are a keystone of sustainable nanotechnology. Naturally derived cellulose nanocrystals (CNCs)[1, 2] fit well into this class of compounds due to the ample availability of the starting material, cellulose, which is the most naturally abundant renewable biopolymer.[3, 4] Over the past decade, CNCs have garnered increasing attention due to their high Young's modulus (similar to steel)[5] and tensile strength, ease of surface modification through external -OH groups, optical transparency, and low density.[6-9] These unique properties create potential applications in the fields of thin films[10, 11], self-assembly[12], nanocomposites[13], biomedical[14-18], electronic[19, 20], food packaging[21], and membranes for separation[22, 23], among others. CNCs are typically needle-shaped crystalline nanomaterials (NMs)[24], commonly produced by sulfuric acid hydrolysis of natural cellulose fiber derived from wood, cotton, algae, bacteria, or marine animals.[25] Depending upon the source of the starting cellulose, CNCs can form four natural polymorphs with distinct chemical and physical properties, explained elsewhere.[9, 26-28]

The synthesis or isolation of CNCs with narrow size distribution (< 5% variability) is of great importance, as their intrinsic properties and applications depend on their spatial dimensions and surface chemical properties.[29, 30] For instance, due to their large surface area and high-negative surface charge [(-37 to -39) mV], drug molecules can be bound to the surface of CNCs, and effective payload and dose control might be achieved by controlling the size of the CNC.[29, 31] Typical CNC dimensions range from about (50 to > 1000) nm in length and from a few nm to a few tens of nm in width/thickness, with the raw (unfractionated) material characteristically highly polydisperse.[32-34]

In the past, researchers developed various synthetic and separation procedures with an objective to yield CNCs with a 'narrow' size distribution, however, the literature in this area is extremely limited. For instance, Bai et al. (2009) reported a differential centrifugation technique, which is capable of fractionating CNCs with 20 nm resolution.[35] Commercial microcrystalline cellulose (MCC) powder was acid-hydrolyzed by sulfuric acid and centrifuged at different angular velocities to separate different fractions. In another study, phase separation of bacterial CNCs in aqueous suspension was investigated;[36] however, the size distribution for each fraction was extremely large (200 nm). Guan et al. (2012) [37] applied asymmetrical-flow field-flow fractionation (AF4) coupled with multi-angle light scattering (MALS) to separate different fractions of CNC. Cotton fabric and MCC were digested with sulfuric acid and purified CNCs were fractionated. The size distributions for all fractions collected at 5 min intervals were in accordance with the transmission electron microscopy (TEM) data.[37] Despite demonstrating the capacity of AF4 for CNC size-fractionation, there are fundamental limitations in this previous study that restrict its application towards practical purposes. For instance, Guan et al. were unable to quantify CNC recovery and molar mass due to insufficient differential refractometry (dRI) signal intensity in their experiments. These two parameters are of great importance: recovery data is critical for assessing the overall efficiency of the fractionation method, while the weight-averaged molar mass (M_w) serves as an absolute characterization parameter for CNCs. Moreover, the reported method was not optimized, other than injection mass, which limits its

usefulness for method application. It is also worth noting that Guan et al. did not evaluate the root mean square radius of gyration (R_g). In a study published after completion of the present work, Ruiz-Palomero et al.,[38] described a liquid-liquid extraction procedure for obtaining CNCs from consumer products like toothpaste, and included AF4 analysis of extracted and prepared CNCs using a programed elution. Although these authors made some effort to optimize the AF4 separation, their analysis was limited, the focus being primarily on comparison of extracted materials and the effect of the extraction process. Molar mass and shape factor were not reported, though CNC length was shown as a function of retention time, and also as cumulative and differential distributions. It is unclear how the authors determined CNC length or converted their programmed fractograms into distributions, as this was not discussed. Alternatively, Hu and Abidi recently demonstrated a pressurized multi-stage filtration approach to obtain a series of narrow size populations, which were then applied in studies of size-dependent nematic self-assembly of the rod-like structures.[30]

Notwithstanding these prior efforts, analytical method optimization and experimental measurements of intrinsic properties for CNCs in situ, e.g., M_w and R_g, as well as preparative methodology, remain largely unexplored.[37] Herein, we demonstrate the use of AF4 coupled to online MALS, dynamic light scattering (DLS), and dRI detectors to fractionate and characterize CNCs. Separation is demonstrated, with collected fractions having a size dispersion at the ± 5 nm level. UV-vis detection was excluded due to the very low molar absorptivity of CNCs (ϵ =0.0546 m^2/mol at 280 nm).

The primary objective of this work was to establish a reproducible optimized AF4 method for CNC fractionation with high recovery (≥ 95 %) and using a surfactant-free mobile phase. This method will facilitate development of CNCs for a broad range of potential applications, which are currently limited by the broad size dispersion of this naturally sourced nanomaterial. For this purpose, separation parameters, e.g., cross flow (V_x), channel flow (V_c), membrane type, injection volume, and focus flow rate, among others, were optimized. The molar mass and shape factor were calculated experimentally, as a function of retention time, using light scattering. Finally, we developed a method for mg-quantity semi-preparatory separation that could potentially be used and further optimized to meet research and industrial needs for high quality, narrow size band CNCs.

Materials and Methods

Reagents

The CNC Certified Reference Material (CNCD-1) was obtained from the National Research Council (NRC), Canada.[39] These CNCs were prepared by sulfuric acid hydrolysis of softwood pulp and exhibit a typical acicular morphology (see Figure S1 in the Electronic Supplementary Material - ESI). Sodium chloride (NaCl, 99+ %) was purchased from Alfa Aesar (Ward Hill, MA)[Ψ] and used as received. An Aqua Solutions (Jasper, GA, USA) Type-II ultra-

[Ψ] The identification of any commercial product or trade name does not suggest endorsement or recommendation by the National Institute of Standards and Technology.

low TOC biological grade water purification system was used to produce the deionized (DI) water (18 MΩ·cm). Mobile phase (NaCl solution) was filtered through a regenerated cellulose filter (0.2 µm) from VWR (Bridgeport, NJ). Stock and working solutions of CNC and NaCl were prepared gravimetrically by dispersing or dissolving the required amount in DI water.

Preparation of CNC dispersion

The CNC stock suspension was prepared in DI water following the protocol prescribed by NRC Canada.[24, 39] Briefly, a probe sonicator (Sonifier 450, Branson Ultrasonics, Danbury, CT) with a ¼" diameter solid titanium immersion probe was used. The sonicator output was first calibrated following a published NIST protocol adopted by NRC Canada.[40, 41] Depending upon the requirements, 200-300 mg of CNCD-1 was placed in a 50 mL polypropylene conical bottom centrifuge tube. The calculated amount of filtered DI water was added to obtain 2 % mass fraction CNC, followed by vigorous shaking to promote dispersion. The mixture was left at room temperature for 24 h. Sonication was carried out by placing the probe at the center of the tube, approximately ½" below the suspension surface and using continuous sonication at setting# S3, which resulted in an average power delivered to the suspension of about 13 W (ESI, Figure S2). During sonication, the 50-mL tube was immersed in a 500-mL glass beaker containing water at ambient temperature (23 ± 1 °C) to avoid excessive heating of the sample. A total of 5000 J/g energy was delivered (at setting# S3) into the CNC suspension. After sonication, the stock suspension was removed and stored at 5 °C for further analysis. For both off-line DLS and on-line AF4 based measurements, desired concentrations were achieved by serially diluting the stock 2 % CNC suspension with DI water and/or 10 mmol/L NaCl as required.

Off-line zeta potential and DLS validation

Off-line measurements of zeta potential (mV), D_h (hydrodynamic diameter derived from cumulants analysis, commonly referred to as Z-average) and polydispersity index (PDI), were performed using a Malvern Zetasizer Nano ZS (Malvern Instruments Inc., Westborough, MA) and following the NRC Canada procedures as reported for CNCD-1.[39] Additionally, the effects of different cuvettes (for D_h) and cells (for zeta potential) were evaluated (see ESI for further details). For both zeta potential and DLS, 0.05 % CNC suspensions were diluted from the stock to a final NaCl concentration of 5 mmol/L. Samples were analyzed within 3 h after preparation, and measurements were performed at 25 °C with values for viscosity and refractive index equal to 0.8872 mPa s and 1.330, respectively. The mean zeta potential was calculated using the Smoluchowski approximation and using monomodal analysis mode.

Sample preparation, AF4 instrumentation, and analysis

An Eclipse3+ (Wyatt Technology, Santa Barbara, CA) AF4 system was used for this study. The system as implemented consisted of a degasser (Gastorr TG-14, Flom Co., Ltd., Tokyo, Japan), an 1100-series isocratic pump (Agilent Technologies, Santa Clara, CA), a long channel (275 mm length, Wyatt Technology), 18 scattering angle MALS detector (Dawn Heleos-II, Wyatt Technology) with a 120-mW laser at 685 nm, a fiber optic DLS detector at a scattering angle of 99° (Wyatt QELS, Wyatt Technology), and a terminal dRI detector (685 nm, Optilab

rEX, Wyatt Technology). The desired quantity of sample (0.1 % mass fraction CNC diluted with DI water from the 2 % stock) was introduced by a 1260 ALS series autosampler from Agilent Technologies. Polyethersulfone (PES) 10 kDa and regenerated cellulose (RC) 10 kDa membranes were purchased from Wyatt Technology. Mylar trapezoidal spacers with 250 µm, 350 µm, and 490 µm nominal thickness (length 26.5 cm and narrowing width from 2.1 to 0.6 cm) were used to establish the nominal channel dimensions. The temperature of the MALS and dRI detectors were maintained at 25.0 ± 0.1 °C, which was within ± 1 ^{o}C of ambient temperature. Prior to each analysis, the dRI detector was purged with mobile phase (NaCl solution) and the baseline set to zero. The blank baseline subtraction procedure was not adopted, as the temperature and solvent flow profiles remained constant throughout each run (i.e., pressure induced baseline shifts were not observed during these experiments). AF4 data was analyzed using OpenLab (Agilent technologies) and Astra 6.1.4.25 (Wyatt Technology) software. The *dn/dc* value (refractive index increment or change of refractive index with change in concentration of the solute) for CNCs was determined by off-line injections (see below) into the dRI, which was then used as a concentration detector. Mass recovery was calculated using Astra software, which multiplies the volume (determined from the flow rate and collection interval) by the concentration (determined from the dRI value and *dn/dc*) for each 'slice' of the eluting peak, then sums these over the selected time interval to obtain the total recovery value; for present purposes, the void peak was excluded from recovery determination, and therefore unretained analyte would be counted as a loss. M_w and R_g were determined using the Zimm model in the Astra software (see Experimental determination of M_w, R_g, and shape factor).

Optimization of the analytical fractionation was performed with an objective to obtain reproducible size separation of CNCs combined with high recovery at concentrations providing suitable sensitivity for the on-line detectors. In addition, a semi-preparatory method was developed to optimize separation of the predominant CNC population (R_h = 25 nm - 40 nm) for off-line analysis and research. Table S1 (in ESI) provides the fractionation parameters selected and used in the optimization process for both analytical and semi-preparatory purposes.

All on-line measurements were performed at 25 ± 0.1 ^{o}C, directly controlled by the MALS, DLS, and dRI detectors. Ambient temperature was within ± 2 ^{o}C of the experimentally controlled temperature.

Determination of *dn/dc*

The dRI detector was used to calculate sample mass concentration and recovery. The *dn/dc* was determined off-line as follows. Four dilutions of the CNC stock, ranging from (0.00125 to 0.01) g/mL, were first filtered through a 0.45 µm PTFE filter and then injected into the Optilab rEX using a Razel syringe pump (model R-99) at a constant flow rate of 0.3 mL/min. This mass concentration range yields a sufficient signal to accurately establish *dn/dc*, which is subsequently measured on-line at local concentrations that are significantly lower, but well above, the baseline. The baseline was determined using a blank consisting of 1 mmol/L NaCl solution. The mean dRI calibration constant (average of two replicate calibration series using NaCl solutions) was 3.5088 $\times 10^{-5}$ refractive index units/pixel.

Uncertainty statement

Unless otherwise stated, all uncertainties reported in this work represent one standard deviation of the mean (± 1 SD) based on 3 to 5 replicate measurements under repeatability conditions.

Results and Discussion

Off-line DLS and zeta potential measurements

CNC dispersions (0.05 % mass fraction) in 5 mmol/L NaCl (i.e., replicating the NRC protocol) yielded D_h ranging from (67 to 69) nm over multiple sample preparations and cell types (ESI, Figure S3), and a PDI from 0.17 to 0.21 (ESI, Figure S4), which are in good agreement with the certified value for D_h of 70.0 ± 1.4 nm and the reported PDI of 0.18.[39] The surface charge of sulfuric acid derived CNCs, and therefore the zeta potential, arises principally from sulfate ester groups on the surface.[2] A mean zeta potential of -38 mV was measured using two different cell types (ESI, Figure S5), which is consistent with the zeta potential reported for informational value on the certificate (-37 mV). The measured pH of test suspensions was 5.0 ± 0.1. For additional details on off-line measurements and a discussion of the potential effects of rotational diffusion, refer to the ESI.

Analytical fractionation

Previously, multidector-AF4 systems have been successfully applied to the fractionation and characterization of nanorods[42, 43] and natural or synthetic polymers.[44, 45] Multi-detector AF4 is also useful for compounds with high molar mass and high branching ratio,[45] and capable of assessing particle morphology by determining the shape factor ρ, which is a ratio of R_g to the mean intensity-weighted equivalent-sphere hydrodynamic radius from DLS cumulants analysis, R_h.[46]

In the current work, initial separation was performed using a constant V_c value of 0.5 mL/min with variable V_x (ESI, Table S1)[47]. Samples were fractionated with PES (250 µm spacer) and RC (350 µm spacer) membranes at (0.1 to 1) mL/min V_x, as required. Upon optimizing the V_x and selecting the appropriate membrane (RC), the V_c, focus flow rate, and sample loading were varied to find the optimal value. Further details are described below.

Effect of membrane composition, cross flow (V_x), and channel flow (V_c)

Generally, PES membranes showed considerably lower reproducibility and sample recovery (26%-79%) for CNCs compared with RC membranes (recovery up to 99 %). Mass recoveries depended slightly on the ionic strength of the mobile phase over the tested range. Differences in recovery were also observed depending upon on whether discrete or continuous injections were used, where discrete refers to DI-blank injections between each sample injection and continuous refers to sample injections with no DI-blank measurement between (see ESI). Both PES and RC membranes showed an increase in sample retention time with increase in crossflow and the ionic strength of the mobile phase at (1 and 5) mmol/L NaCl. On the other hand, 0.1 mmol/L mobile phase showed negligible variation in retention time with both [PES (12

± 0.1) min at V_x = (0.2 - 0.5) mL/min] and RC (13.1 ± 0.1 min at V_x = 0.4 - 0.8 mL/min) membranes.

Results show that the recovery with PES membrane is considerably lower than RC membrane with some exceptions. For instance, with continuous runs (i.e., without intermediate blank injections), recoveries with PES exceeded 95 % at low crossflow of 0.1 mL/min and for lower mobile phase ionic strength [(0.1 and 1) mmol/L)]. From the standpoint of effective fractionation, however, these conditions are not very useful as the total peak width is only ≈ 10 mins, from which fractions with low size dispersion (< ± 5 nm) cannot be collected. The higher recoveries obtained from continuous runs compared to discrete runs may imply that CNCs adhere onto the PES membrane causing a memory effect. However, the actual reason for the relatively poor performance by PES membranes (under optimal separation conditions) is not fully understood at this time. Inconsistent behavior of RC membranes has also been occasionally observed, even with membranes from the same lot/batch. For instance, some RC membranes were observed to foul faster than others. This not only results in poor recovery, but also decreases reproducibility. Although this warrants caution while working with RC membranes, RC membranes were determined to be the best overall choice for CNC separation based on observed recovery and fractionation behavior. RC was therefore chosen as the membrane for optimization of CNC fractionation and all parameters were optimized using continuous injections as described above, in order to maximize reproducibility and recovery.

The optimization of V_x was performed by maintaining V_c at 0.5 mL/min, while V_x was varied from (0.6 - 1.0) mL/min.[47] Results show that within this range, all V_x are sufficient to retain the CNCs throughout the elution run (Figure 1); the size distribution of CNCs across the main peak remained similar independent of V_x. Peak retention time shifted towards longer times as V_x increased, i.e., 9.0 ± 0.6 min at 0.6 mL/min, 11.8 ± 0.1 min at 0.8 mL/min, and 13.9 ± 0.1 min at 1.0 mL/min (Figure 1), while recoveries were found to be near 90 % across this range. Therefore, a mid-value V_x of 0.8 mL/min was selected for further optimization. Next, we optimized the channel flow by holding V_x at 0.8 mL/min. Results show a small void peak at 4.5-5 min when V_c = 0.7 mL/min. However, due to the relatively small quantity of unretained CNCs, the overall recovery was not significantly affected. Unlike V_x, V_c showed little impact on CNC mass recovery (94.1 % to 96.2 %) over the range V_c = (0.3 - 0.5) mL/min. However, the overall sample fractionation showed significant effects due to channel flow. At high V_c (0.7 mL/min), the CNC distribution is overly condensed. This is also suggested by the larger void peak compared with other runs, indicating the presence of a relatively large unretained CNC fraction in the void peak. It should be noted that optimal retention behavior, based on CNC size-fractionation, occurred at V_c = 0.3 mL/min. However, the total elution time was more than 70 min, which is substantially longer than that at V_c = 0.5 mL/min. Therefore, considering the combination of analyte recovery, total elution time, and elimination of coelution effects, V_c = 0.5 mL/min was determined to be the optimal channel flow rate for CNC separation.

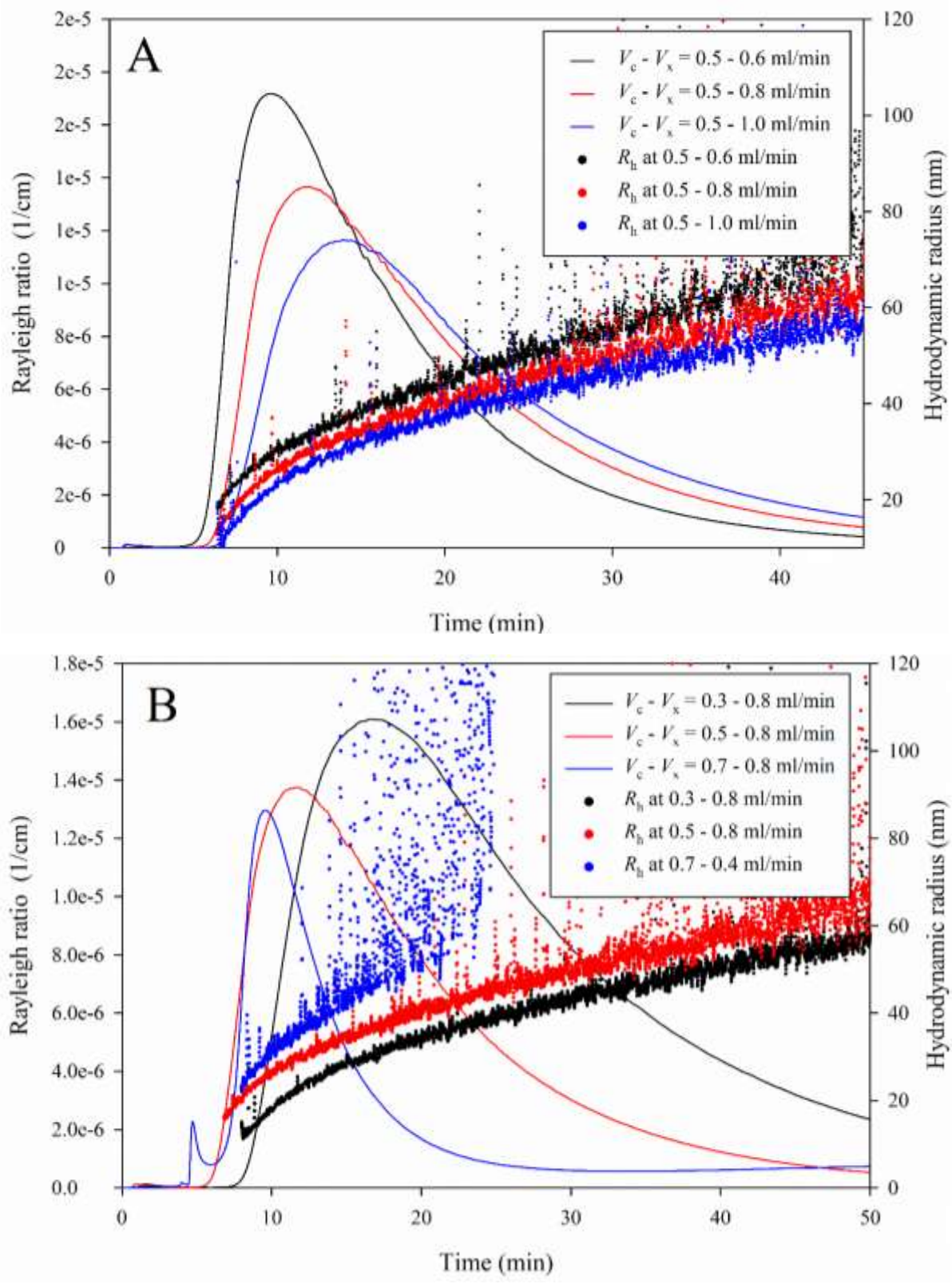

Figure 1. AF4 fractograms at (A) 0.5 mL/min V_c and variable V_x [(0.6-1.0) mL/min)] and (B) 0.8 mL/min V_x and variable V_c [(0.3-0.5) mL/min] with 1.0 mmol/L NaCl as mobile phase for CNCs. Solid lines are $R(\Theta)$ from MALS scattering intensity measured a scattering angle of 90°.

Effect of mobile phase composition, sample load and focus flow rate

Studies conducted by the NRC showed that the dispersion stability of CNC in dilute (5 mmol/L) NaCl solution at ± 4 °C was up to a month.[39] Based on this information, NaCl solution was selected as the mobile phase for optimization. Moreover, no surfactant (e.g., sodium dodecyl sulfate, Triton X, etc.) was used to enhance the retention behavior of the CNCs, because their presence can complicate the process of recovering pure CNCs from the solution phase and surfactants produce a complex mobile phase that can interfere with on-line analysis. With a dilute NaCl mobile phase, fractions can be collected and used for additional off-line characterization and/or applications. Use of pure DI water as a mobile phase was tested, but did not produce acceptable separation (data not shown), likely due to the absence of sufficient charge screening, which can lead to poor retention behavior.[48 49]

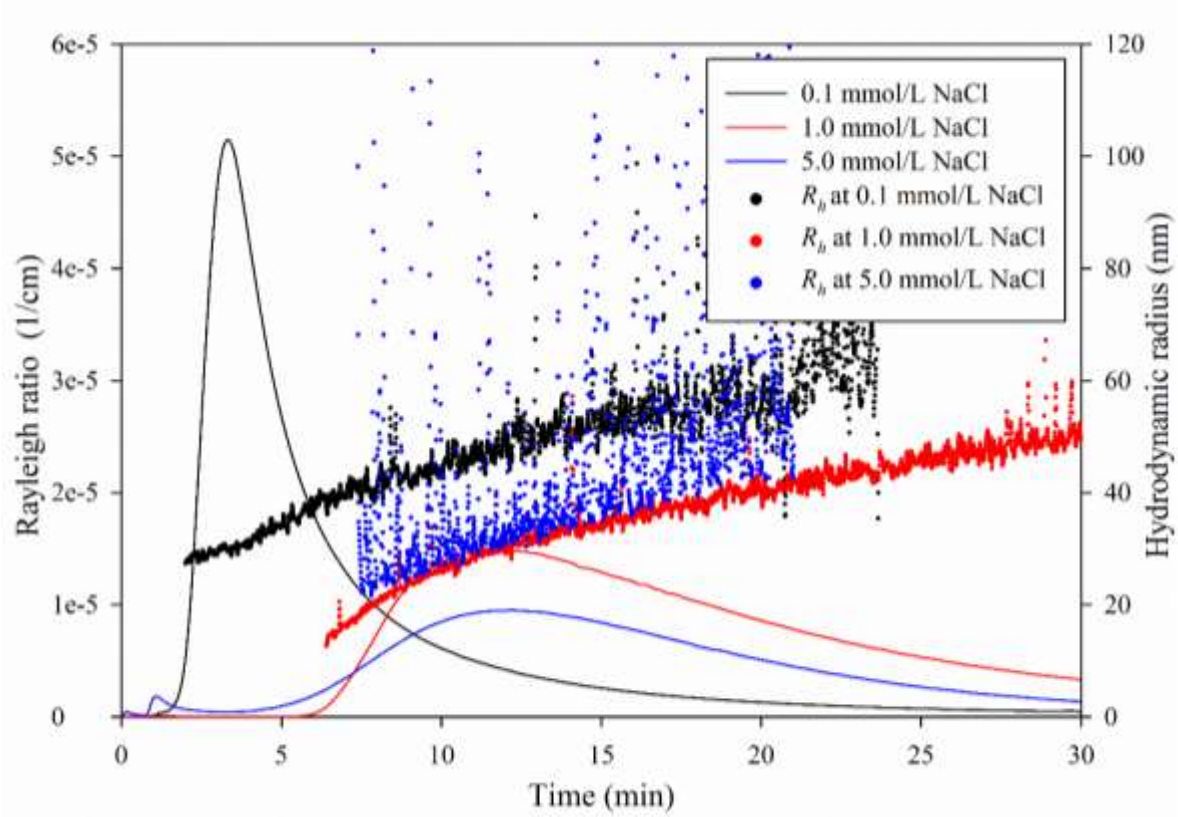

Figure 2. AF4 fractograms at $V_c - V_x$ = (0.5 - 0.8) mL/min with (0.1, 1.0, and 5.0) mmol/L NaCl as mobile phase for CNCs. Solid lines are $R(\Theta)$ obtained from MALS measured at a scattering angle of 90 °.

Among the three NaCl concentrations tested, i.e., (0.1, 1.0, and 5.0) mmol/L, 1 mmol/L exhibited the combination of recovery and size dispersion throughout the run. Recovery was found to be > 96 % with 1 mmol/L NaCl at V_c = 0.5 mL/min and V_x = 0.8 mL/min (Figure 2), depending on the sample quantity injected. Additionally, the noise in the data is clearly minimal for 1.0 mmol/L. In Figure 2, a shift in R_h values is apparent upon the initial increase in salt concentration, i.e., from (0.1 to 1.0) mmol/L NaCl. This is attributed, at least in part, to the shift (elongation) in the overall retention profile to which these values are associated. Considering the

non-linear relationship and variability of R_h values with elution time, an average value would not provide insight. Note that at 0.1 mmol/L the size distribution is more compressed toward the initial part of the elution, but the noise level increases toward the last part of the elution due to the low concentration of analyte in the detection zone. The elution profile observed at 5 mmol/L is similar to 1 mmol/L, but the noise level for R_h values remained very high across the entire run, suggesting strong interactions with the membrane and lower recovery. At 1 mmol/L, a reasonable size dispersion (over roughly 25 min elution time) was achieved with relatively low noise. Notably, M_w values varied from (9.6 to 11.6) x 10^7 Da over the same range in mobile phase ionic strength; values that are within the expected range (vida infra). Within this concentration range, 1 mmol/L NaCl was selected for the mobile phase to achieve the optimal combination of separation and recovery.

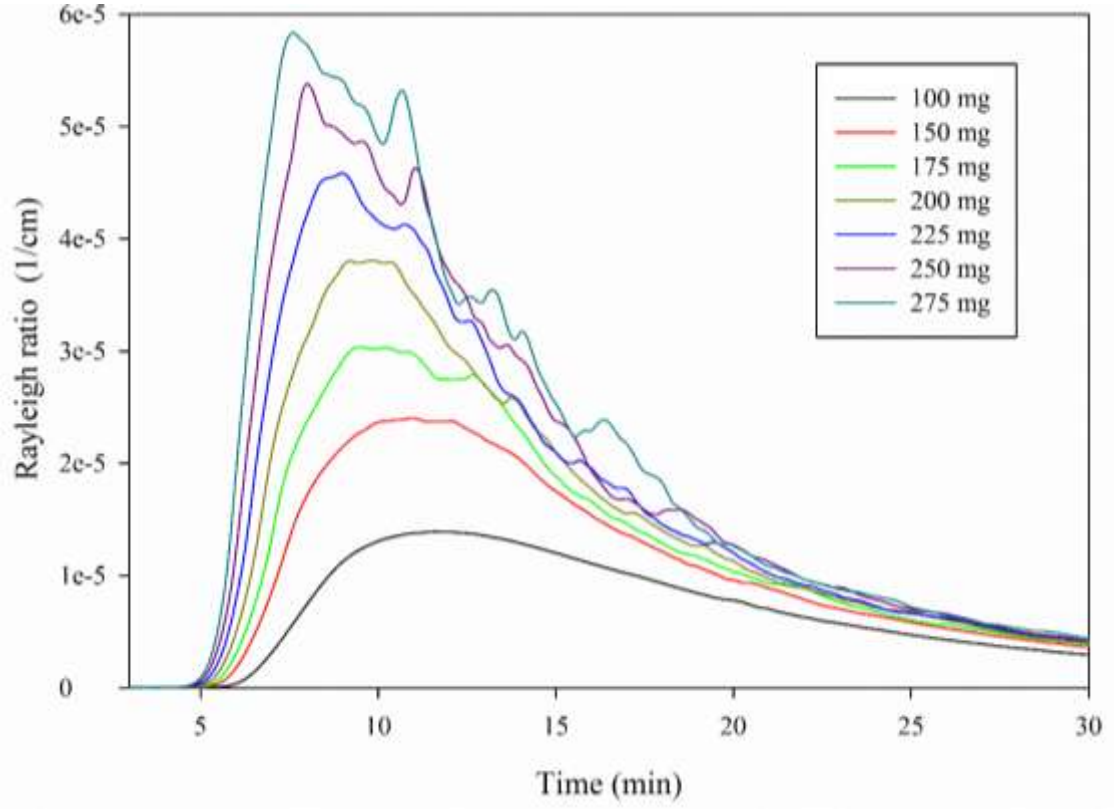

Figure 3. AF4 fractograms at V_c-V_x = (0.5 - 0.8) mL/min and mobile phase 1.0 mmol/L NaCl as a function of sample load. Solid lines are $R(\Theta)$ obtained from MALS measured at a scattering angle of 90 °.

The effect of sample load on recovery was evaluated by injecting (100 to 275) µg of CNC (Figure 3), wherein injection volume was varied to obtain the desired load. Over the tested mass range, recovery did not vary considerably. Recovery reached a maximum of ≈ 99 % at 150 µg sample injection. Further increase in sample load decreased recovery slightly to a low of 96.6 %; a value above 95 % is considered excellent recovery from an analytical standpoint. Although sample load does not appreciably impact recovery here, the onset of sample

overloading is suggested by the degradation in quality of the MALS data above 150 µg (Figure 3), and becomes substantial with sample load > 225 µg. In the case of channel overloading, coelution of larger and smaller CNCs is expected (as species are forced into the faster streamlines of the parabolic flow above the channel center), as well as other phenomena that may manifest as noisy scattering signals. Based on these measurements, the sample load should be kept below 200 µg with V_c-V_x = (0.5 – 0.8) mL/min in 1 mmol/L NaCl mobile phase.

Experimental determination of M_w, R_g, and shape factor

After optimization of the instrumental parameters following our previously reported protocol[47], M_w and R_g were calculated using the Astra software based on a form of the Debye-Zimm relationship[50] (Figure 4). Molar mass determination by light scattering is documented elsewhere.[51] Briefly, the light scattering intensity of particles and macromolecules in a liquid medium has an angular dependence if the scatters are sufficiently large (R_g of order 30 nm). The M_w and R_g were calculated by using the following equation[52, 53]:

$$\frac{K^*c}{R(\theta)} = \frac{1}{M_w} + \frac{16\pi^2}{3\lambda^2}\frac{1}{M_w}(R_g)^2 Sin^2\left(\frac{\theta}{2}\right) \qquad \text{Eq. (1)}$$

Here $R(\theta)$ is the excess Rayleigh ratio (representing the scattering intensity at angle θ relative to the incident intensity in excess of the solvent scattering),[54] K^* is a constant ($= \frac{4\pi^2 n_0^2}{N_A\lambda^4}\left(\frac{dn}{dc}\right)^2$), c is the analyte concentration in g/mL, λ is the wavelength of incident light, N_A is Avogadro's number and n_0 is the refractive index of the medium. The intercept and the slope of the plot $\frac{K^*c}{R(\theta)}$ vs $Sin^2\left(\frac{\theta}{2}\right)$ gives $\frac{1}{M_w}$ and $\frac{16\pi^2}{3\lambda^2}\frac{1}{M_w}(Rg)^2$, respectively, from which M_w and R_g can be calculated during on-line measurements. Another important physical property can be determined from R_g and R_h, known as the Burchard-Stockmayer shape parameter, $\rho = R_g/R_h$.[46] Depending upon the measured ρ values, the shape of the analyte can be estimated. For example, the theoretical value of ρ for a hard sphere is 0.778 and for thin stiff rods it is 2.36; ρ for ellipsoids ranges from 0.875 to 0.987 for oblate and from 1.36 to 2.24 for prolate.[55] This relationship can be used as a proxy for shape in the case of CNCs. Our findings (1.5 to 1.9) are clearly within the prolate ellipsoid-to-rod regime. Previously published TEM and AFM results (see also ESI, Figure S1), suggest that CNCD-1 is needle-shaped, with some tendency to form lateral associations.[24]

The average M_w and R_g of the fractions eluted within the first 40 min was (11,498 ± 546) kDa and (63 ± 19) nm, respectively (Figure 4). During elution, both M_w and R_g increased with increasing R_h. The experimental M_w value is consistent with an estimated value of 10^4 kDa calculated in a previous study for CNC dimensions of 150 nm x 10 nm and an assumed density (not reported, but 1.5 g/cm^3 is a widely accepted value for cellulose)[37]. The mean ρ value for CNCD-1 (averaged over all data points between (6 and 30) min retention time) was 1.43 ± 0.08 (Figure 4); above 30 min and below 6 min, data quality and reliability are reduced significantly due to the low number of CNCs present in the extremes of the eluting peak – this data is therefore truncated. Comparatively, the slope of a linear fit to R_g versus R_h (ESI, Figure S6)

yields a value of 1.49. Notably, ρ is nearly constant across the main peak of eluting CNCs shown in Figure 4. This value is lower than expected for needle or thin rod structures, and could be attributed to lateral aggregates, either preexisting or formed during the AF4 focusing step. The latter scenario seems unlikely due to the consistency of ρ across the peak. R_g and R_h increase continuously with retention time across the eluted CNC peak, while the shape factor is roughly constant. This suggests that fractionation produces size separation of individual CNCs or laterally associated bundles with increasing length, thereby greatly reducing the polydispersity inherent to these materials.

Theoretically, rod length can be calculated during fractionation using the MALS data applied to a cylindrical scattering model and assuming the particles meet the criteria for the Rayleigh-Gans approximation for weak scatterers. Details of the scattering theory and its application to CNCs is described elsewhere.[37, 56] For comparison to the mean length values reported on the CNCD-1 certificate,[39] rod length was calculated as a function of retention time using the rod form factor model provided with the on-board Astra software (see ESI, Figure S7). The rod model requires an assumed value for radius, a, or that $a << L$ (i.e., a=0). Similarly, for long thin rigid rods, the simple relation $R_g^2 \approx L^2/12$ can be applied.[56] Using this relationship and applying to R_g values at the peak FWHM limits in Figure 4, the calculated rod length varies from about (101 to 204) nm; the peak maximum rod length is 146 nm. These values coincide closely with the results obtained using the rod form factor model (with a slowly increasing deviation as R_g increases, see Figure S7), but are approximately 2-fold larger than the mean lengths reported on the CNCD-1 certificate based on AFM (76 nm) and TEM (87) measurements.[39] Notably, the length range obtained by light scattering in the present study is similar to that found previously by Guan et al. for two sources of CNCs.[37] Though an in depth analysis of the light scattering calculations is beyond the scope of the present work, it is worth noting that substituting realistic values for a in the rod model had no effect on the calculated length; similarly, calculations using R_g but restoring the second term containing the rod radius ($R_g^2 = L^2/12 + a^2/2$) were equally insensitive to a for realistic values over the FWHM of the peak (less than a 1 % difference). The lack of agreement between microscopy and light scattering suggests that the cylindrical model may not be appropriate for CNCD-1 or that deposition and counting during microscopic analysis is not sufficiently capturing the longer rod populations. This issue requires further attention, but lies outside the scope of the present work.

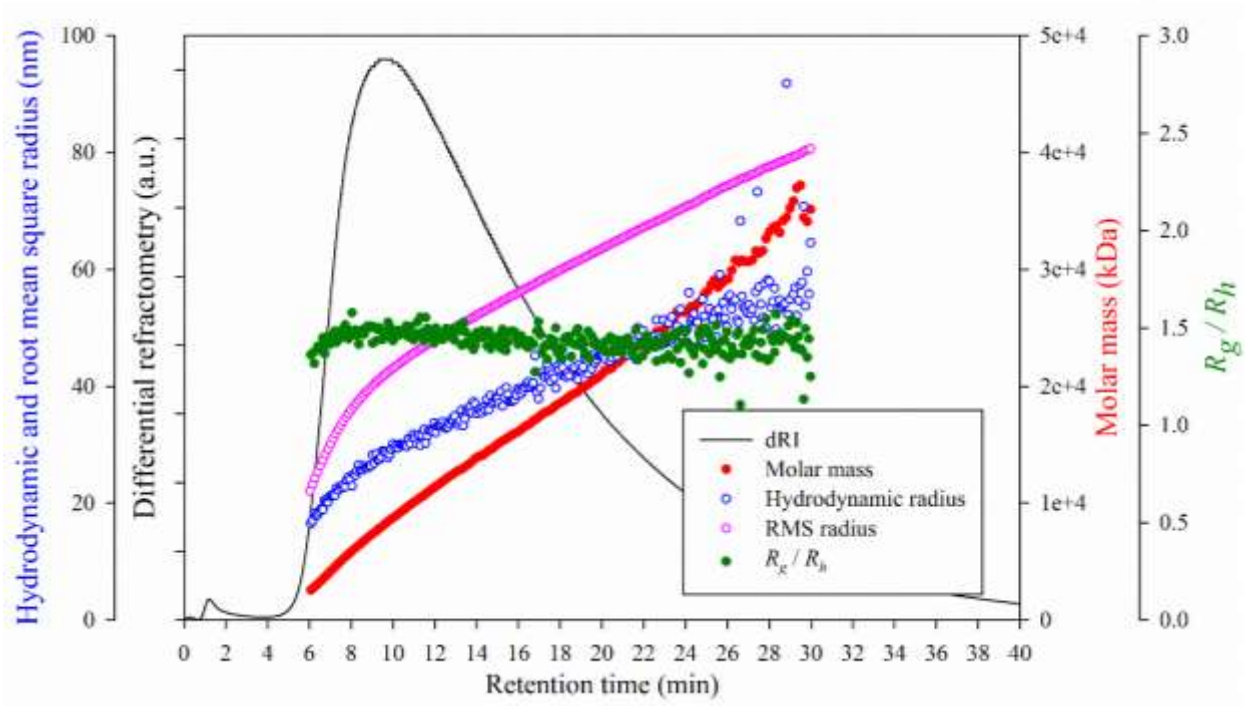

Figure 4. Representative fractogram and Burchard-Stockmayer plot for CNCD-1 showing the variation of weight-average molar mass (MALS derived, Da), R_g nm, R_h nm and shape parameter R_g/R_h with retention time up to 30 min measured on-line during AF4 fractionation. Black line shows the dRI trace. Data above 30 min and below 6 min has been truncated due to low analyte concentration. For all data except dRI, a sampling rate from 10 to 20 was used to improve visibility.

Optimized fractionation conditions

The analytical fractionation was performed by injecting 100 µg of CNC dispersed in 1 mmol/L NaCl with a 350 µm Mylar spacer and 10 kDa MWCO RC membrane at V_c = 0.5 mL/min and V_x = 0.8 mL/min (see Table 2 for a summary of optimal AF4 parameters). In a typical fractogram (ESI, Figure S8), fractions were collected online during two-minute intervals. Analysis results for these fractions are summarized in Table 1. The elution profile was divided into 12 equal fractions (F1 to F12), starting at 5 min (F1) and up to 29 min (F12), as most of the CNC mass was eluted during that time period. Results show that the average molar mass of all the fractions together was 13,516 kDa, but the standard deviation is 6855, which is almost 50 % of the mean value (Table 1). A high standard deviation is due to the high polydispersity observed and, therefore, the average M_w of the CNC dispersion should not be considered as a true experimental value for M_w. On the other hand, small fractions show acceptable standard deviations (< 2 %) and the PDI = M_w/M_n [ratio of weight and number average molar mass calculated in ASTRA] ranged from 1.000 - 1.072 for all individual fractions, which is essentially monodisperse. The average hydrodynamic radius for the entire population (all fractions collectively) also showed high standard deviation (≈ 27 % of the mean value) due to polydispersity. Therefore, mean DLS

results for batch (unfractionated) CNCs should be used with caution while considering the accuracy of particle size in the presence of substantial polydispersity.

Table 1. Molar mass (M_w), hydrodynamic radius (R_h), and mass recovery for each collected fraction (F1-12) identified in the fractogram shown in Figure S7 (see ESI).

Fractions	M_w (kDa)	R_h (nm)	Mass recovery (%)
Global average	13,516 ± 6855	35.5 ± 9.6	89.4 ± 5.0
F1	1446 ± 27	18.3 ± 2.3	3.3 ± 0.2
F2	3720 ± 81	21.0 ± 0.4	14.9 ± 0.3
F3	6590 ± 107	26.2 ± 0.3	16.6 ± 0.1
F4	9156 ± 98	30.0 ± 0.3	13.7 ±0.1
F5	11461 ± 95	33.1 ± 0.4	10.6 ± 0.1
F6	13,479 ± 102	35.7 ± 0.2	8.1 ± 0.1
F7	15,254 ± 122	38.0 ± 0.3	6.3 ± 0.1
F8	16873 ± 93	40.5 ± 0.5	4.9 ± 0.0
F9	18,480 ± 112	42.4 ± 0.2	3.8 ± 0.0
F10	20,207 ± 219	45.2 ± 0.7	3.0 ± 0.0
F11	21,943 ± 163	46.7 ± 1.2	2.3 ± 0.0
F12	23,582 ± 125	48.8 ± 0.8	1.9 ± 0.0

Semi-preparatory fractionation

The goal here was to isolate the major fraction (R_h = 25 nm - 40 nm) of CNC by maximizing the sample load in the shortest time possible without substantially compromising the recovery. Therefore, increase in channel flow (V_c) and application of lower cross flow (V_x) are two of the primary parameters to be optimized. From the analytical separation, we conclude that RC membrane (10 kDa cutoff) is the better choice over PES with ≈ 99 % recovery. Hence, the RC membrane was also adopted for the semi-preparatory separation. The spacer used for analytical purposes had a thickness of 350 µm. To accommodate a higher sample load inside the channel, a 490 µm spacer was used for the semi-preparatory separation. The mobile phase was 1 mmol/L NaCl as this gave us the best recovery previously.

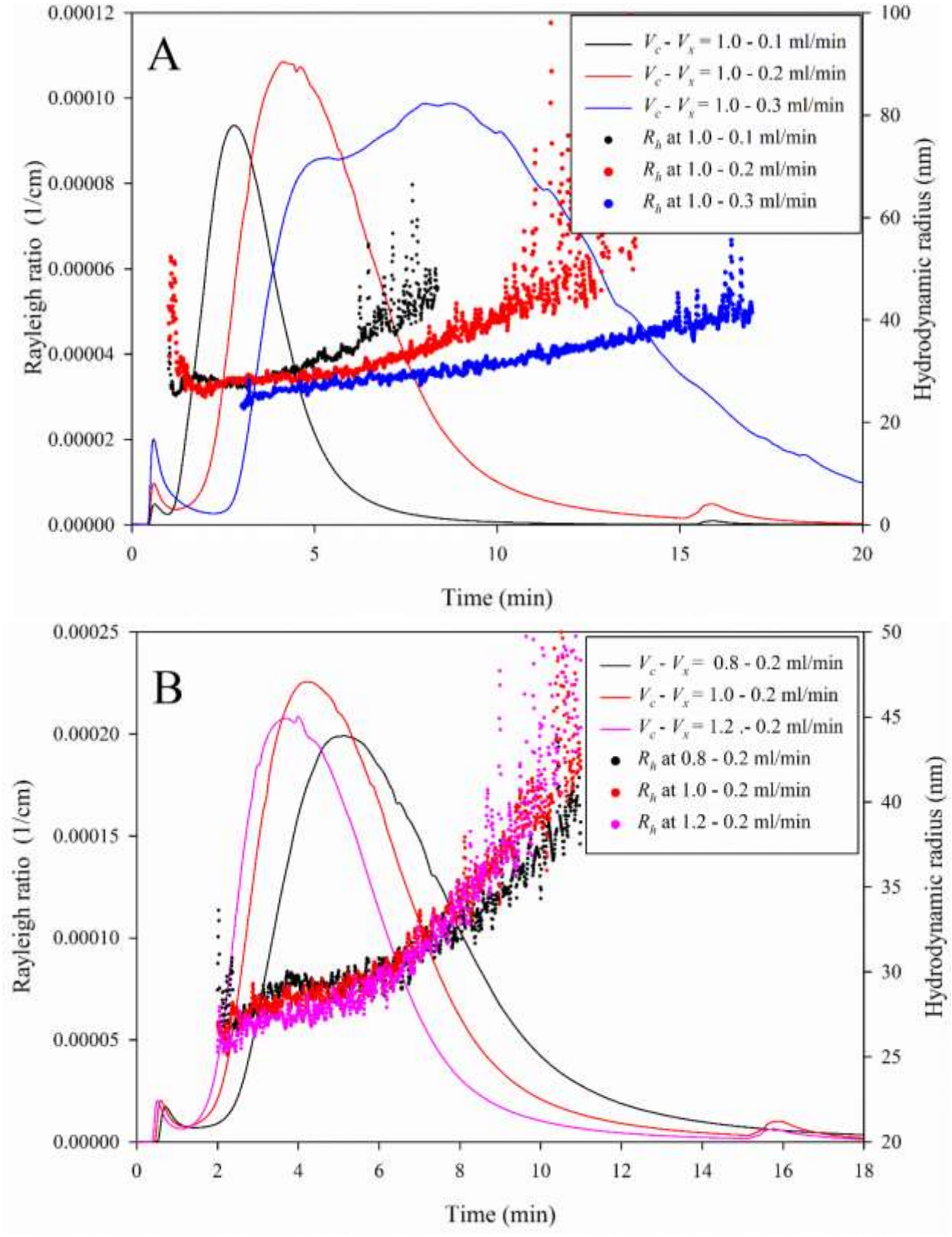

Figure 5. AF4 fractograms at (A) 1.0 mL/min V_c and variable V_x [(0.1 - 0.3) mL/min)] and (B) 0.2 mL/min V_c and variable V_d [(0.8 - 1.2) mL/min] with 1.0 mmol/L NaCl as mobile phase for CNCs. Solid lines represent MALS intensity traces measured at a scattering angle of 90 °.

Initially, V_c was set to 1 mL/min. The sample load was increased up to 10× compared to the analytical separation, injecting 1 mg CNC per run. Under these conditions, V_x values of (0.1, 0.2, and 0.3) mL/min were tested. Results show that both (0.1 and 0.2) mL/min yielded acceptable size fractionation as a function of elution time. However, at 0.3 mL/min, CNC-membrane interactions begin to impact fractionation (Figure 5A). The spread of CNC fractions at V_x = 0.1 mL/min was considerably smaller than 0.2 mL/min, which made it difficult to isolate the R_h = 25 nm to 40 nm fraction, due to the coelution of larger particles. Therefore, 0.2 mL/min crossflow was used for semi-preparatory separation.

Upon optimizing V_x, V_c was varied from (0.8 to 1.2) mL/min to find the most suitable channel flow (Figure 5B). All three V_c values exhibited similar fractions with a slight drop in the recovery (≈ 2 %) at 0.8 mL/min. Negligible variation in overall fractionation, sample retention, and mass recovery (94.5 % - 94.7 %) were observed at V_c of (1.0 and 1.2) mL/min. Therefore, 1.0 mL/min was selected as the optimum V_c for further analysis.

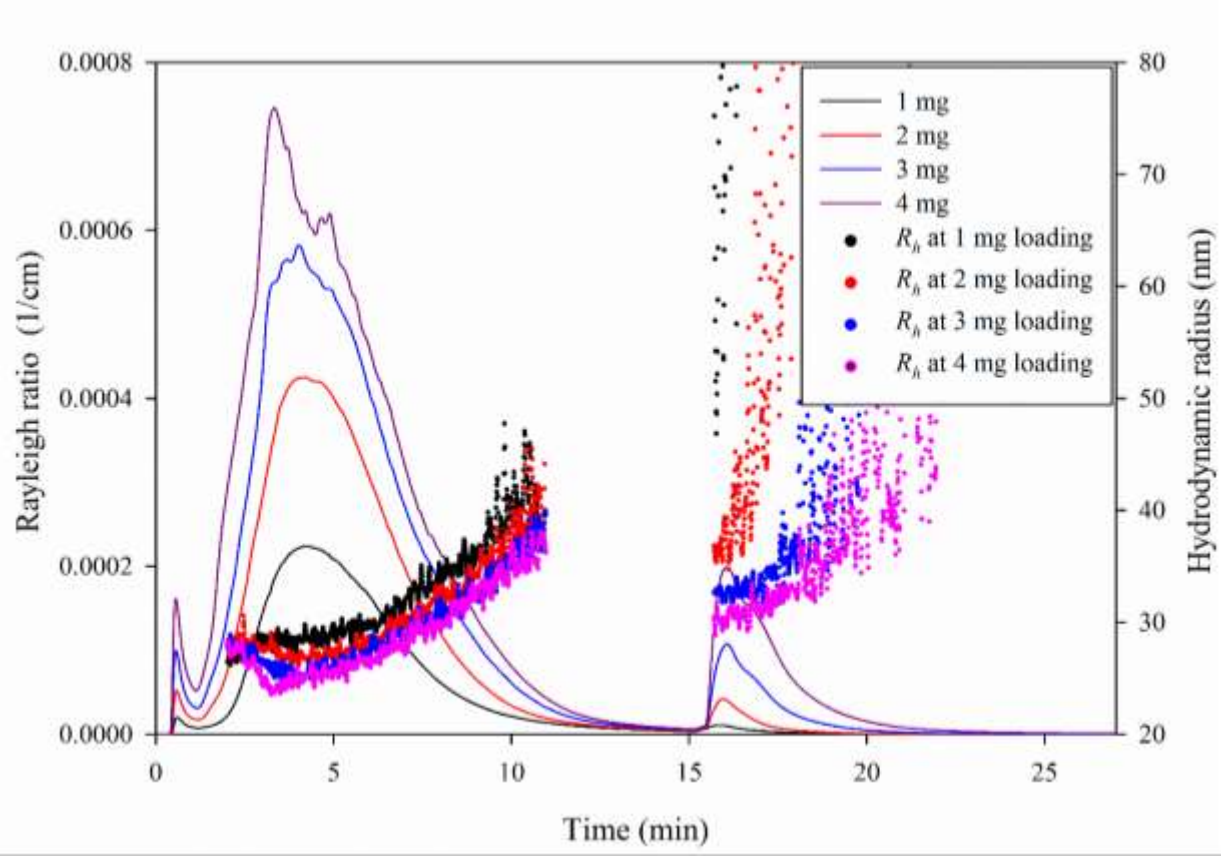

Figure 6. AF4 fractograms at V_c 1.0 mL/min and V_x = 0.2 mL/min, with mobile phase 1.0 mmol/L NaCl and as a function of sample load. Solid lines represent MALS intensity traces measured at a scattering angle of 90 °. Peaks appearing after 15 min retention time result from field release and are expected to contain a mixture of sizes.

Next, sample loading was optimized. Injections of (1 to 4) samples were made, which were (10 to 40) times higher than the analytical method. The mass recovery was greater than 90 % (91.3 % to 93.2 %) with (1 – 2) mg sample injection. However, recovery decreased (83 % - 87.7 %) with further increase in loading. The average R_h values for fractions collected between (2 and 11) min remained almost unaltered (26.9 nm – 30.2 nm), as did the molar mass (98,035 kDa – 10,769 kDa). To examine material lost during this fractionation, the field release peak eluted when V_x dropped to zero (at 15 min) was analyzed. Results indicate that the (25 – 40) nm fraction eluted during the first (2 -10) min with a 1 mg sample injection; i.e., the field release peak (after 15 min in Figure 6) is nearly absent. The R_h values for the release peaks are too noisy to be meaningful, due to the low concentration of CNCs present and the lack of separation (i.e., coelution). However, loss of analyte increased with an increase in sample loading above 1 mg, and reached 9 % of the total mass at 4 mg. Moreover, an indication of membrane overloading (distorted MALS trace) became apparent at 3 mg and was prominent at 4 mg (Figure 6). Therefore, 2 mg was determined to be the maximum sample loading acceptable under these conditions, with analyte mass recovery around 1.8 mg within 11 mins of elution.

Focus flow and focus time were varied from (1 to 3) mL/min and from (1 to 3) min, respectively, with no significant effects on CNC fractionation observed (data not shown). Therefore, a 1 min focusing time was used to minimize the overall fractionation time.

The average value of the shape factor for (R_h = 25 nm – 40 nm) nm fraction was found to be 1.9 ± 0.1, which is consistent with a rod-like shape (ESI, Figure S9). The overall optimized conditions are listed in Table 2.

Table 2. Optimized AF4 parameters used for analytical and semi-preparatory fractionation of CNCs.

		Analytical fractionation	**Preparatory fractionation**
Channel parameters	Membrane	RC	RC
	Membrane cut-off	10 kDa	10 kDa
	Spacer	350 µm	490 µm
Flow rates	Injection flow	0.2 mL/min	0.2 mL/min
	Channel flow (V_c)	0.5 mL/min	1.0 mL/min
	Cross flow (V_x)	0.8 mL/min	0.2 mL/min
Sample loading	Injection amount	100 – 200 µg	2 - 3 mg
Time parameters (as sequenced in the method)	1) Elution	2 min	30 sec
	2) Focus	2 min	30 sec
	3) Focus + Injection	3 min	2 min
	4) Focus	3 min	1 min
	5) Elution	60 min	10 min

Conclusions

AF4 with multi-detection was evaluated and optimized for the analytical size-based separation and on-line characterization of naturally derived polymeric cellulose nanocrystals (CNCs), with an objective to produce fractions containing narrow size-distributions (< 5 nm) with minimal perturbation of the analyte and maximal recovery. In this study, multi-angle light scattering (MALS), dynamic light scattering (DLS) and differential refractometry (dRI) were utilized on-line to determine the weight-averaged molar mass, radius of gyration, hydrodynamic radius and the shape factor for fractionated CNCs in a mobile phase containing dilute NaCl. Despite low signals produced by the dRI detector, we successfully determined the *dn/dc* value for CNC (0.148 ± 0.003 mL/g), thereby providing on-line mass quantification for recovery determinations. The only previously published determination of *dn/dc* for CNCs reported a value of 0.126 g/L.[38] Even assuming the units were reversed, this is a factor of 1000 off from the present value and from the generally accepted value for proteins (0.190 mL/g),[57] calling into question their *dn/dc* results and the recoveries derived thereby.

Using MALS data (excess Rayleigh ratio) and the Zimm relationship, the root mean square radius or radius of gyration and molar mass were calculated. R_h was measured using a fiber optic coupled DLS device. The shape factor was determined from the ratio R_g/R_h. The average shape factor for analytical and semi-preparatory analysis ranged from 1.5 to 1.9, which falls within the prolate ellipsoid-to-rod-like range, and did not change appreciably with retention time. The experimentally determined weight averaged molar mass was consistent with a reported estimate of 10^4 kDa. Results show that the best fractionation and recovery are achieved with a mobile phase ionic strength of 1 mmol/L NaCl. This is a critical parameter in order to achieve desired separation and good mass recovery. Optimized fractionation resulted in high recoveries (up to 99 %) and excellent separation of CNCs. Moreover, the absence of surfactants in the mobile phase during fractionation makes this a green separation technique, which preserves the pristine chemical composition of the CNC fractions throughout the separation and quantification process. Finally, an optimized semi-preparatory separation method was developed and evaluated, which can generate ≈10 mg of CNCs with R_g = (25 – 40) nm in one hour. Future work should be directed towards optimized method development for surface modified CNCs, improvement in preparative methodology for higher throughput with narrow size dispersion and orthogonal analysis of the morphology and aggregation state of fractionated CNC (including the appropriateness of existing light scattering models).

Conflicts of interest

There are no conflicts of interest to declare.

Acknowledgements

The authors thank Dr. Linda Johnston (NRC-Canada) for providing the certified reference material CNCD-1 used in this study, for access to methods and data obtained by NRC on batch samples, and for useful discussions regarding CNC dispersion and characterization. We acknowledge NRC-Canada for providing the TEM image of CNCD-1 reproduced with their

permission in the ESI. We also thank Dr. John Pettibone of NIST for manuscript review and useful feedback, and Dr. Jeremie Parot of NIST for useful discussions regarding the application of the rod form factor model.

References

1. K. Kummerer, J. Menz, T. Schubert and W. Thielemans, *Chemosphere*, 2011, **82**, 1387-1392.
2. D. Klemm, F. Kramer, S. Moritz, T. Lindström, M. Ankerfors, D. Gray and A. Dorris, *Angewandte Chemie International Edition*, 2011, **50**, 5438-5466.
3. R. M. Domingues, M. E. Gomes and R. L. Reis, *Biomacromolecules*, 2014, **15**, 2327-2346.
4. J. George and S. N. Sabapathi, *Nanotechnology, science and applications*, 2015, **8**, 45-54.
5. F. L. Dri, L. G. Hector, R. J. Moon and P. D. Zavattieri, *Cellulose*, 2013, **20**, 2703-2718.
6. L. Groom, L. Mott and S. Shaler, *Wood Fiber Sci*, 2002, **34**, 14-27.
7. S. J. Eichhorn, A. Dufresne, M. Aranguren, N. E. Marcovich, J. R. Capadona, S. J. Rowan, C. Weder, W. Thielemans, M. Roman, S. Renneckar, W. Gindl, S. Veigel, J. Keckes, H. Yano, K. Abe, M. Nogi, A. N. Nakagaito, A. Mangalam, J. Simonsen, A. S. Benight, A. Bismarck, L. A. Berglund and T. Peijs, *J Mater Sci*, 2010, **45**, 1-33.
8. R. R. Lahiji, X. Xu, R. Reifenberger, A. Raman, A. Rudie and R. J. Moon, *Langmuir*, 2010, **26**, 4480-4488.
9. R. J. Moon, A. Martini, J. Nairn, J. Simonsen and J. Youngblood, *Chem. Soc. Rev.*, 2011, **40**, 3941-3994.
10. L. Csoka, I. C. Hoeger, O. J. Rojas, I. Peszlen, J. J. Pawlak and P. N. Peralta, *Acs Macro Lett*, 2012, **1**, 867-870.
11. J. D. Fox, J. R. Capadona, P. D. Marasco and S. J. Rowan, *Journal of the American Chemical Society*, 2013, **135**, 5167-5174.
12. T. Nypelo, C. Rodriguez-Abreu, Y. V. Kolen'ko, J. Rivas and O. J. Rojas, *Acs Applied Materials & Interfaces*, 2014, **6**, 16851-16858.
13. A. E. Hess, J. R. Capadona, K. Shanmuganathan, L. Hsu, S. J. Rowan, C. Weder, D. J. Tyler and C. A. Zorman, *J Micromech Microeng*, 2011, **21**, 054009 (9pp).
14. A. Shimotoyodome, J. Suzuki, Y. Kumamoto, T. Hase and A. Isogai, *Biomacromolecules*, 2011, **12**, 3812-3818.
15. G. Helenius, H. Backdahl, A. Bodin, U. Nannmark, P. Gatenholm and B. Risberg, *J Biomed Mater Res A*, 2006, **76A**, 431-438.
16. R. A. N. Pertile, S. Moreira, R. M. G. da Costa, A. Correia, L. Guardao, F. Gartner, M. Vilanova and M. Gama, *J Biomat Sci-Polym E*, 2012, **23**, 1339-1354.
17. N. Ferraz, D. O. Carlsson, J. Hong, R. Larsson, B. Fellstrom, L. Nyholm, M. Stromme and A. Mihranyan, *J R Soc Interface*, 2012, **9**, 1943-1955.
18. N. Lin, A. Geze, D. Wouessidjewe, J. Huang and A. Dufresne, *Acs Applied Materials & Interfaces*, 2016, **8**, 6880-6889.
19. Y. Okahisa, A. Yoshida, S. Miyaguchi and H. Yano, *Compos Sci Technol*, 2009, **69**, 1958-1961.
20. S. Rajala, T. Siponkoski, E. Sarlin, M. Mettanen, M. Vuoriluoto, A. Pammo, J. Juuti, O. J. Rojas, S. Franssila and S. Tuukkanen, *Acs Applied Materials & Interfaces*, 2016, **8**, 15607-15614.
21. D. Trache, M. H. Hussin, C. T. Hui Chuin, S. Sabar, M. R. Fazita, O. F. Taiwo, T. M. Hassan and M. K. Haafiz, *Int J Biol Macromol*, 2016, **93**, 789-804.
22. S. A. Paralikara, J. Simonsen and J. Lombardi, *J Membrane Sci*, 2008, **320**, 248-258.
23. Z. Karim, A. P. Mathew, M. Grahn, J. Mouzon and K. Oksman, *Carbohyd Polym*, 2014, **112**, 668-676.
24. A. Brinkmann, M. H. Chen, M. Couillard, Z. J. Jakubek, T. Y. Leng and L. J. Johnston, *Langmuir*, 2016, **32**, 6105-6114.
25. D. Bondeson, A. Mathew and K. Oksman, *Cellulose*, 2006, **13**, 171-180.

26. A. C. OSullivan, *Cellulose*, 1997, **4**, 173-207.
27. Y. Nishiyama, *J Wood Sci*, 2009, **55**, 241-249.
28. I. A. Sacui, R. C. Nieuwendaal, D. J. Burnett, S. J. Stranick, M. Jorfi, C. Weder, E. J. Foster, R. T. Olsson and J. W. Gilman, *ACS Appl Mater Interfaces*, 2014, **6**, 6127-6138.
29. S. Kalia, A. Dufresne, B. M. Cherian, B. S. Kaith, L. Averous, J. Njuguna and E. Nassiopoulos, *Int J Polym Sci*, 2011, 837875.
30. Y. Hu and N. Abidi, *Langmuir*, 2016, **32**, 9863-9872.
31. A. Taheri and M. Mohammadi, *Chem Biol Drug Des*, 2015, **86**, 882-886.
32. S. Beck-Candanedo, M. Roman and D. G. Gray, *Biomacromolecules*, 2005, **6**, 1048-1054.
33. S. Elazzouzi-Hafraoui, Y. Nishiyama, J.-L. Putaux, L. Heux, F. Dubreuil and C. Rochas, *Biomacromolecules*, 2008, **9**, 57-65.
34. Y. Habibi, L. A. Lucia and O. J. Rojas, *Chem Rev*, 2010, **110**, 3479-3500.
35. W. Bai, J. Holbery and K. C. Li, *Cellulose*, 2009, **16**, 455-465.
36. A. Hirai, O. Inui, F. Horii and M. Tsuji, *Langmuir*, 2009, **25**, 497-502.
37. X. Guan, R. Cueto, P. Russo, Y. D. Qi and Q. L. Wu, *Biomacromolecules*, 2012, **13**, 2671-2679.
38. C. Ruiz-Palomero, M. Laura Soriano and M. Valcárcel, *Microchim Acta*, 2017, **184**, 1069-1076.
39. National Research Council Canada, CNCD‑1: Cellulose Nanocrystal Powder Certified Reference Material, Certificate of Analysis, http://www.nrc-cnrc.gc.ca/eng/solutions/advisory/crm/certificates/cncd_1.html.
40. J. S. Taurozzi, V. A. Hackley and M. R. Wiesner, *Nanotoxicology*, 2011, **5**, 711-729.
41. J. S. Taurozzi, V. A. Hackley and M. R. Wiesner, *NIST Special Publication*, 2012, **1200**.
42. J. Gigault, T. J. Cho, R. I. MacCuspie and V. A. Hackley, *Analytical and Bioanalytical Chemistry*, 2013, **405**, 1191-1202.
43. T. Nguyen, J. Liu and V. Hackley, *Chromatography*, 2015, **2**, 422.
44. I. Tugel, J. R. Runyon, F. G. Galindo and L. Nilsson, *J I Brewing*, 2015, **121**, 44-48.
45. T. Otte, H. Pasch, T. Macko, R. Brull, F. J. Stadler, J. Kaschta, F. Becker and M. Buback, *Journal of Chromatography A*, 2011, **1218**, 4257-4267.
46. W. Burchard, M. Schmidt and W. H. Stockmayer, *Macromolecules*, 1980, **13**, 1265-1272.
47. J. Gigault, J. M. Pettibone, C. Schmitt and V. A. Hackley, *Anal Chim Acta*, 2014, **809**, 9-24.
48. T. Rameshwar, S. Samal, S. Lee, S. Kim, J. Cho and I. S. Kim, *Journal of nanoscience and nanotechnology*, 2006, **6**, 2461-2467.
49. D. H. Kim, J. Moon and J. Cho, *J Water Supply Res T*, 2005, **54**, 249-259.
50. B. H. Zimm, *J Chem Phys*, 1948, **16**, 1093-1099.
51. P. Debye, *The Journal of physical and colloid chemistry*, 1947, **51**, 18-32.
52. M. Andersson, B. Wittgren and K. G. Wahlund, *Anal Chem*, 2003, **75**, 4279-4291.
53. P. J. Wyatt, *Anal Chim Acta*, 1993, **272**, 1-40.
54. A. D. McNaught, A. Wilkinson and International Union of Pure and Applied Chemistry., *Compendium of chemical terminology : IUPAC recommendations*, Blackwell Science, Oxford England ; Malden, MA, USA, 1997.
55. A. K. Brewer and A. M. Striegel, *Analyst*, 2011, **136**, 515-519.
56. P. J. Wyatt, *Anal. Chem.*, 2014, **86**, 7171-7183.
57. H. Zhao, Patrick H. Brown and P. Schuck, *Biophysical Journal*, 2011, **100**, 2309-2317.